Hairless regulates heterochromatin maintenance and muscle stem cell function as a histone demethylase antagonist

Ling Liu[a,1], Cristina Rodriguez-Mateo[a], Polly Huang[a], Albin Huang[a], Alexander Lieu[a], Michelle Mao[a], Mingyu Chung[a], Sharon Yang[a], Kevin Yu[a], Gregory W. Charville[a,b], Qiang Gan[a], and Thomas A. Rando[a,c,1]

[a]Paul F. Glenn Center for the Biology of Aging, Department of Neurology and Neurological Sciences, Stanford University School of Medicine, Stanford, CA 94305; [b]Department of Pathology, Stanford University School of Medicine, Stanford, CA 94305; and [c]Neurology Service and Rehabilitation Research and Development Center of Excellence, Veterans Affairs Palo Alto Health Care System, Palo Alto, CA 94304

Edited by Eric N. Olson, University of Texas Southwestern Medical Center, Dallas, TX, and approved July 26, 2021 (received for review December 28, 2020)

Skeletal muscle possesses remarkable regenerative ability because of the resident muscle stem cells (MuSCs). A prominent feature of quiescent MuSCs is a high content of heterochromatin. However, little is known about the mechanisms by which heterochromatin is maintained in MuSCs. By comparing gene-expression profiles from quiescent and activated MuSCs, we found that the mammalian Hairless (Hr) gene is expressed in quiescent MuSCs and rapidly down-regulated upon MuSC activation. Using a mouse model in which Hr can be specifically ablated in MuSCs, we demonstrate that Hr expression is critical for MuSC function and muscle regeneration. In MuSCs, loss of Hr results in reduced trimethylated Histone 3 Lysine 9 (H3K9me3) levels, reduced heterochromatin, increased susceptibility to genotoxic stress, and the accumulation of DNA damage. Deletion of Hr leads to an acceleration of the age-related decline in MuSC numbers. We have also demonstrated that despite the fact that Hr is homologous to a family of histone demethylases and binds to di- and trimethylated H3K9, the expression of Hr does not lead to H3K9 demethylation. In contrast, we show that the expression of Hr leads to the inhibition of the H3K9 demethylase Jmjd1a and an increase in H3K9 methylation. Taking these data together, our study has established that Hr is a H3K9 demethylase antagonist specifically expressed in quiescent MuSCs.

muscle stem cells | heterochromatin | aging

Skeletal muscle in adult animals has remarkable regenerative capacity because of the resident muscle stem cells (MuSCs), or satellite cells. Electron microscopic examination reveals that MuSCs are characterized by compact heterochromatin and a very thin layer of cytoplasm (1). In response to muscle damage, MuSCs activate, reenter the cell cycle, and give rise to myogenic progenitors that express the myogenic transcription factor MyoD1 (2). Recent findings suggest that chromatin condensation is a mechanism to regulate the myogenic progression of MuSCs. Histone 4 Lysine 20 trimethylation (H4K20me3) is a histone mark often associated with heterochromatin formation. In quiescent MuSCs, H4K20me3 was found at the promoter region of MyoD1 and deletion of the H4K20 methyltransferase Suv4-20h-1 is associated with premature expression of MyoD1 in quiescent MuSCs and a depletion of these cells (3). However, the functional importance of heterochromatin maintenance at a genome-wide level in quiescent MuSCs remains largely unexplored.

A hallmark of heterochromatin is trimethylation of histone 3 lysine 9 (H3K9me3). H3K9me3 is required for transcriptional silencing of a large number of genes (4, 5). The compact structure of H3K9me3-enriched heterochromatin plays an important role in maintaining genome integrity. Loss of H3K9 methylation is associated with increased DNA damage in heterochromatic regions and the activation of cell cycle checkpoint pathways in both somatic and germ cells of *Drosophila* (6). Furthermore, the activation of ataxia telangiectasia mutated (ATM) kinase and double-strand break repair can be blocked by methylation of H3K9 (7), further suggesting the importance of H3K9 methylation and heterochromatin integrity in genome maintenance.

Histone methylation is maintained by a balance between specific methyltransferases and demethylases. The H3K9 demethylase Jmjd1a (also known as Kdm3a) was first cloned as a male germ cell-specific gene from rats and is indispensable for androgen receptor signaling and normal spermatogenesis (8, 9). It has also been shown to be critical for the self-renewal of embryonic stem cells (10). The expression of Jmjd1a is prominent in MuSCs and remains constant throughout cell activation and lineage progression (11, 12). Transcriptional regulation of Jmjd1a has been studied in various cell types. Jmjd1a is a target gene of Oct4 in embryonic stem cells and appears to be a target of microRNA-22 in Ewing's sarcoma cells (13). In addition, Jmjd1a has been found to be regulated by phosphorylation in response to heat shock in Jurkat lymphoma cells (14). However, the posttranscriptional regulation of Jmjd1a activity remains largely unknown.

In the present study, we find that the Jumonji family member Hairless (Hr) is expressed in quiescent MuSCs and is rapidly down-regulated when MuSCs are activated to enter the cell cycle. By generating a mouse in which Hr is conditionally ablated in MuSCs, we demonstrate that the expression of Hr in MuSCs ensures normal MuSC-mediated muscle regeneration. Following acute muscle injury, Hr depletion leads to a reduction in the number of self-renewed MuSCs. Loss of Hr in adult MuSCs leads to a reduction in genome-wide H3K9me3 levels, increases the susceptibility of these cells to genotoxic stress, leads to increased cell death upon activation from quiescence, and accelerates the

Significance

Skeletal muscle stem cells (MuSCs) exhibit a high content of heterochromatin. However, little is known about the functional importance of heterochromatin maintenance in MuSC homeostasis. Our study uncovered the role of the Hairless (Hr) gene in protecting the integrity of heterochromatin in MuSCs. We characterized the molecular function of Hr and demonstrated its role as an antagonist to Histone 3 Lysine 9 demethylases. Our work has implications for the importance of heterochromatin maintenance in stem cell function during aging.

Author contributions: L.L. and T.A.R. designed research; L.L., C.R.-M., P.H., A.H., A.L., M.M., M.C., S.Y., K.Y., G.W.C., and Q.G. performed research; L.L., C.R.-M, P.H., and M.C. analyzed data; and L.L. and T.A.R. wrote the paper.

The authors declare no competing interest.

This article is a PNAS Direct Submission.

[1]To whom correspondence may be addressed. Email: lingliu@stanford.edu or rando@stanford.edu.

This article contains supporting information online at https://www.pnas.org/lookup/suppl/doi:10.1073/pnas.2025281118/-/DCSupplemental.

Published September 7, 2021.

loss of these stem cells during aging. In addition, we demonstrate that Hr functions as an antagonist to the H3K9 demethylase Jmjd1a. The expression of Hr maintains normal H3K9me3 levels and heterochromatin structure in MuSCs, demonstrating the importance of heterochromatin maintenance in stem cell function and homeostasis.

Results

Hr Is Specifically Expressed in Quiescent MuSCs. In mammalian cells, the methylation state of H3K9 is maintained by the balance between the SET domain-containing methyltransferases and the Jumonji domain-containing demethylases (15). Together, these histone-modifying enzymes maintain proper heterochromatin demarcation and configuration. In order to understand how H3K9 methylation is regulated in quiescent MuSCs, we used microarray and RNA-sequencing (RNA-seq) analysis of MuSCs from uninjured skeletal muscle and from skeletal muscle 2.5 d after injury to identify H3K9 methyltransferases or demethylases that are specifically expressed in the quiescent state (11, 12). Despite a lack of change in the overall levels of H3K9me2 and H3K9me3 in MuSCs upon activation (*SI Appendix*, Fig. S1*A*), the expression of regulators of H3K9 methylation changes dynamically. While a number of H3K9 methyltransferases—including Suv39h1, Suv39h2, Setdb1, Setdb2, Ehmt1, and Ehmt2—increase expression in activated MuSCs, we found that a few H3K9 demethylases, including Kdm7a and Jmjd1c, as well as a putative demethylase Hr, were more highly expressed in quiescent MuSCs than in activated MuSCs (*SI Appendix*, Fig. S1*B*). Within the group of H3K9 regulators that are down-regulated upon MuSC activation, Hr showed the greatest differential expression. We confirmed by qRT-PCR the expression of Hr in quiescent MuSCs and its dramatic down-regulation upon activation (*SI Appendix*, Fig. S1*C*). In skeletal muscle, Hr expression is also detected in resident fibro-adipogenic progenitors (*SI Appendix*, Fig. S1*D*). Furthermore, we confirmed the presence of Hr protein in quiescent MuSCs in vivo by immunohistochemical staining of muscle cryosections (Fig. 1*A*).

To further test whether Hr expression correlates with MuSC quiescence, we assessed the percentage of actively proliferating MuSCs and the level of Hr expression at different time points after muscle injury. To quantify the percentage of proliferating MuSCs, we administered EdU by intraperitoneal injection prior to MuSC isolation by fluorescence-activated cell sorting (FACS). Isolated cells were either plated to allow for detection of EdU by immunofluorescence or used for qRT-PCR analysis of Hr expression levels. We found that greater than 70% MuSCs and their progeny were in the cell cycle 3 d after muscle injury and that this percentage had declined to about 20% 1 wk after the injury (Fig. 1*B*). Interestingly, Hr expression was found at the lowest level in MuSCs 3.5 d after injury, coinciding with the peak of proliferation of MuSC progeny, and returned to the level found in quiescent MuSCs 2 wk after injury when proliferation of MuSC progeny has essentially ceased (Fig. 1*B*). The expression of Hr follows the same pattern of the quiescent MuSC marker Pax7, and is the opposite of myogenin, a marker of differentiated myoblasts (Fig. 1*C*). In addition, we found that progeny of MuSCs propagated in culture did not express detectable levels of Hr (*SI Appendix*, Fig. S1*E*). Expressing Hr in myoblasts in culture led to a marked reduction in proliferation (*SI Appendix*, Fig. S1*F*). Taken together, these data indicate that Hr expression is specific to the quiescent state of MuSCs.

Loss of Hr Impairs MuSC Activation and Muscle Regeneration. In order to understand the function of Hr in quiescent MuSCs in vivo, we generated a mouse strain in which exons 7–9 of the Hr gene had been flanked by loxP sites (Fig. 2 *A* and *B*). The disruption of Hr expression in skin is known to lead to hair regeneration defects (16). To confirm the functional ablation of Hr from the floxed alleles, we crossed the Hr floxed mice with a

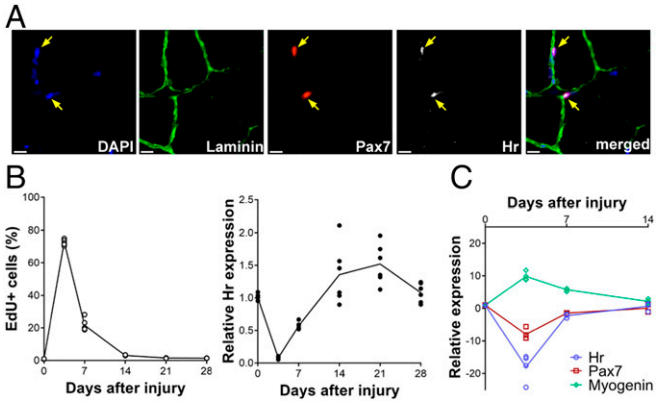

Fig. 1. Hr expression in MuSCs. (*A*) Immunofluorescence staining of Hr in MuSCs in vivo. Cross-sections of TA muscles were stained with antibodies specific to Hr, Pax7, and laminin, confirming the expression of Hr in quiescent MuSCs. MuSCs are marked by arrows. (Scale bars, 10 μm.) (*B*) Percentage of EdU$^+$ cells (*Left*) and Hr expression (*Right*) in MuSCs at different time points after $BaCl_2$ injury. MuSCs and their progeny were isolated by FACS from uninjured mice or from mice at the indicated time points postinjury ($n = 6$). For all time points, mice were injected with EdU every 12 h the day before collection. Cells were then used for EdU detection by immunofluorescence or assessment of Hr expression by qRT-PCR. (*C*) Changes in the expression of Hr and myogenic factors in MuSCs or myogenic progenitors during muscle regeneration. MuSCs and their progeny were isolated 3.5, 7, and 14 d after $BaCl_2$ injury. The expression of Hr and myogenic factors were assessed by qRT-PCR and compared to that in MuSCs from uninjured muscle.

Krt14^{CreER} strain to generate progeny in which Hr expression is specifically ablated in epidermal progenitors (17). We found that 3 mo after the ablation of Hr expression, these mice started exhibiting prominent hair loss in the head (*SI Appendix*, Fig. S2*A*). When we plucked hair from the back of these animals, we found negligible hair regrowth up to 14 d after hair removal, at which time control mice had fully regrown their hair (*SI Appendix*, Fig. S2*A*). The hair regeneration defect in these mice confirmed that our targeting strategy sufficiently abrogated the expression and function of Hr in vivo.

To induce Hr ablation specifically in MuSCs, we crossed the Hr floxed mice with a Pax7^{CreER} strain in which inducible Cre recombinase is expressed only in MuSCs (18). We also crossed the mice with a ROSA26^{eYFP} line in which a stop-floxed YFP allele is introduced into the Rosa26 locus (19) to facilitate the isolation of MuSCs in which the Cre-dependent recombination has occurred. In doing so, we generated Pax7$^{CreER/+}$;ROSA26$^{eYFP/+}$;Hr$^{fl/fl}$ (referred to as "Hr cKO" [Hr conditional knockout] hereafter) mice in which the administration of Tamoxifen (Tmx) induces the ablation of Hr and the expression of YFP as a reporter specifically in MuSCs (*SI Appendix*, Fig. S2*B*). We have confirmed that exons 1–6 of the *Hr* gene does not lead to the accumulation of partial transcripts (*SI Appendix*, Fig. S2*C*), and Hr proteins are not detected in MuSCs isolated from the Hr cKO mice (*SI Appendix*, Fig. S2*D*). To determine whether loss of Hr leads to disruption of MuSC quiescence in vivo, we administered EdU to Hr cKO and control mice for 1 wk and found no difference in the percentage of EdU-incorporated MuSCs (*SI Appendix*, Fig. S2*E*), indicating that MuSCs do not spontaneously enter the cell cycle in the absence of Hr expression. We also quantified the number of MuSCs on single myofibers isolated from the extensor digitorum longus muscle 1, 2, and 4 wk following Tmx injections and found no difference in MuSC number between Hr cKO and control mice (*SI Appendix*, Fig. S2*F*).

In order to determine whether Hr regulates MuSC function and muscle regeneration, we injured the tibialis anterior (TA) muscles of Hr cKO and control mice with barium chloride ($BaCl_2$) and quantified the regenerating area 4 d after injury. We

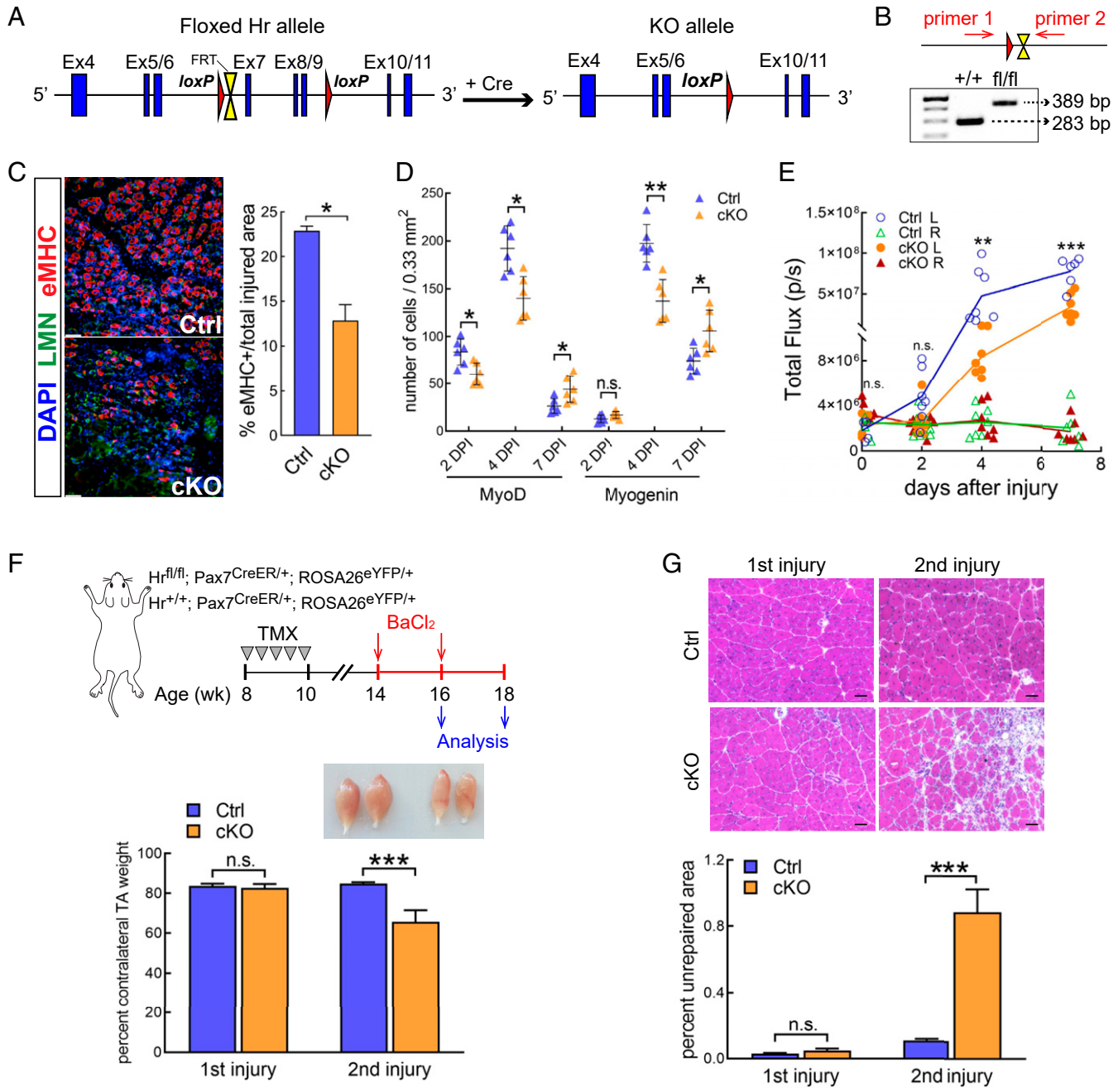

Fig. 2. Delayed MuSC activation and impaired muscle regeneration in Hr cKO mice. (*A*) Schematic representation of the floxed Hr allele before and after recombination. (*B*) Regions selected for genotyping primers and PCR confirmation of the wild-type and floxed Hr allele. (*C*) Comparison of muscle regeneration in Hr cKO and control mice ($n = 3$). Cross-sections were collected from the TA muscles of Hr cKO and control mice 4 d after injury. Newly regenerated myofibers were identified by an antibody specific to embryonic myosin heavy chain (eMHC). (Scale bars, 50 μm.) The eMHC$^+$ area normalized by total injured area is plotted. (*D*) Quantification of MyoD- and Myogenin-expressing cells in Hr cKO and control mice after injury. Muscle cross-sections were collected from Hr cKO or control mice 2, 4, and 7 d after $BaCl_2$ injury. The number of cells expressing MyoD or myogenin were detected using specific antibodies and quantified. (*E*) MuSC activation kinetics in Hr cKO and control mice. The left TA muscles of Hr cKO-Luc ($n = 7$) or control ($n = 6$) mice were injured and the mice were subjected to BLI prior to and 2, 4, and 7 d after injury. The total flux from both TA muscles of each mouse is plotted. (*F*) Loss of muscle weight of Hr cKO mice after repeated injury. Hr cKO or control mice were injured in the left TA muscles once ($n = 5$) or twice ($n = 4$). Both the left and right TA muscles were harvested 1 wk after injury and weighed. The percentage of the weight of the injured TA to that of the contralateral uninjured TA was calculated and plotted. (*G*) Impairment in muscle regeneration in Hr cKO mice after repeated injury. Cross-sections were obtained from the injured TA muscles collected in (*F*) and analyzed by H&E staining. (Scale bars, 50 μm.) The area that is devoid of myofibers was quantified in ImageJ and the ratio between this area and total cross section area was calculated and plotted. Data are shown as mean ± SEM; $*P < 0.05$, $**P < 0.01$, $***P < 0.001$ (unpaired *t* tests).

found fewer and smaller fibers expressing the regenerating marker embryonic myosin heavy chain in the Hr cKO mice (Fig. 2*C* and *SI Appendix*, Fig. S2*G*). Consistent with this, we found a reduction in the number of myogenic progeny of MuSCs 2 and 4 d after injury (Fig. 2*D* and *SI Appendix*, Fig. S2*H*). Interestingly, although the number of MyoD$^+$ and Myogenin$^+$ cells are decreased in Hr cKO mice in comparison to control mice 4 d after injury, the presence of MyoD$^+$ and Myogenin$^+$ cells persist

longer in Hr cKO animals. To investigate the kinetics of MuSC activation in vivo, we generated $Pax7^{CreER/+}$;$ROSA26^{Luc/+}$;$Hr^{fl/fl}$ (referred to as "cKO-Luc" hereafter) mice in which the administration of Tmx induces the ablation of Hr and the expression of firefly luciferase as a reporter specifically in MuSCs (18). We injured the left TA muscle of Hr cKO-Luc and control mice and monitored these mice 2, 4, and 7 d after injury by bioluminescent imaging (BLI). While the luciferase activity in the uninjured legs in both cKO-Luc and control mice remained unchanged, the luminescent intensity of the injured legs was two- to threefold lower in the cKO-Luc mice compared to control mice up to 7 d following injury (Fig. 2*E*), indicating a decreased number of MuSC progeny in cKO-Luc mice. We isolated MuSC progeny from these animals after the last imaging and cultured them in differentiation conditions for 7 d. We then quantified the percentage of cells expressing MHC and found no defect in the ability of Hr-null cells to undergo myogenic differentiation (*SI Appendix*, Fig. S2*I*). These data indicate that the loss of Hr impairs the expansion of MuSC progeny but has no effect on myogenic differentiation.

Despite the impairment in the early phase of regeneration in these animals (*SI Appendix*, Fig. S2 *J–L*), we did not observe a difference in the weight of the regenerated TA muscles or their gross morphology 14 d after injury (Fig. 2 *F* and *G*). However, when we performed sequential injury of the Hr cKO and control mice, we found that a second injury led to significant weight loss of the TA muscles and an accumulation of fibrotic tissues at the injured area in Hr cKO mice (Fig. 2 *F* and *G*). Taken together, these data demonstrate that loss of Hr results in an impairment in the expansion of myogenic progeny from quiescent MuSCs upon their activation, leading to a delay in MuSC-mediated muscle regeneration.

Hr-Null MuSCs Are Defective in Self-Renewal. As muscle regenerates, progeny of MuSCs self-renew to replenish the stem cell pool. We observed that, 4 wk after muscle injury, the number of $Pax7^+$ cells decreased in regenerated muscles of Hr cKO mice (Fig. 3*A*). To confirm the loss of MuSCs in Hr cKO mice following muscle injury, we performed injury and reinjury experiments and quantified the number of YFP^+ cells by FACS 4 wk after each injury. We found about 20% reduction in the number of YFP^+ cells in the TA muscles of cKO mice in comparison to control mice after one injury, and a 36% reduction after the second injury (Fig. 3*B*). While the pool of MuSCs in control mice remained relatively constant after sequential injuries, those in Hr cKO mice were gradually depleted. We confirmed that all YFP^+ cells in these TA muscles express Pax7 by immunofluorescence (*SI Appendix*, Fig. S3 *A* and *B*). These data demonstrate that the loss of Hr impairs the ability of MuSCs to self-renew during muscle regeneration.

We next performed transplantation studies to determine whether the impairment in self-renewal of Hr cKO MuSCs is due to cell-autonomous defects. We mixed luciferase-expressing control or cKO MuSCs with YFP-expressing wild-type MuSCs prior to transplanting them into the TA muscles of recipient NOD-SCID mice whose hindlimbs had been irradiated (Fig. 3*C*). We monitored the recipient mice with BLI immediately and 2, 4, and 7 d after transplantation to assess the intrinsic functionality of the luciferase-expressing control and cKO cells (Fig. 3*C*). At the completion of the studies, the number of YFP-expressing wild-type cells in each muscle was quantified by FACS to ensure equal transplantation efficacy between the two TAs of each recipient that were engrafted with control or cKO MuSCs, and the analysis confirmed no difference between the groups (*SI Appendix*, Fig. S3*C*). The BLI analysis revealed a 40% reduction in the luminescence signal in the TA muscles that were transplanted with cKO cells 4 and 7 d after transplantation (Fig. 3*C*). These results demonstrate that loss of Hr renders MuSCs intrinsically less functional than the control cells.

To test whether the loss of Hr leads to a defect in the process of MuSC activation, we injured muscles of Hr cKO and control mice and then administered EdU. We found Hr ablation led to a three- to fourfold reduction in the number of MuSCs that had incorporated EdU 1 and 2 d after injury (Fig. 3*D*), suggesting an impairment in MuSC activation. We also isolated MuSCs from uninjured Hr cKO and control mice and allowed them to activate ex vivo in the presence of EdU. Consistent with the previous finding, a lower percentage of Hr-null cells incorporated EdU 24 and 48 h after isolation in comparison to control cells (*SI Appendix*, Fig. S3*D*), suggesting that the impairment in MuSC activation in Hr cKO mice results from intrinsic changes in these cells, independent of environmental stimuli. Consistent with this, when we cultured individual myofibers ex vivo, we found a reduction in the number of myogenic progeny attached to myofibers from Hr cKO mice 2 and 3 d after plating (*SI Appendix*, Fig. S3*E*).

Hr-Null MuSCs Are Susceptible to Cell Death upon Activation. We previously showed that, in old animals, the impairment of MuSC replenishment following muscle regeneration is due to the increased susceptibility of MuSCs upon activation to a form of cell death termed mitotic catastrophe (20). Given that the impairment of both muscle regeneration and MuSC self-renewal in Hr cKO mice resembles that in old mice, we sought to determine whether Hr-null MuSCs are more prone to cell death upon activation. We injured the muscles of cKO and control mice and harvested activated MuSCs and their myogenic progeny 3 d after injury. Dead cells were labeled with propidium iodine (PI) and quantified by FACS. This analysis revealed a two- to threefold increase in the number of activated MuSCs that were dying in vivo in cKO animals compared to controls (Fig. 4*A*). In addition, we plated MuSCs isolated from Hr cKO and control mice for time-lapse microscopy. Over the subsequent days, we quantified the percentage of cells that successfully completed cytokinesis and the percentage of cells that underwent cell death. We found that MuSCs of Hr cKO mice were more than two times more likely to undergo cell death compared to control cells (Fig. 4*B*). Analysis of the time-lapse data also revealed that the time-of-death of cKO cells coincided with their time to first division (*SI Appendix*, Fig. S4*A*), suggesting that the Hr cKO cells die by mitotic catastrophe upon activation.

In order to investigate the cellular processes that lead to the increased susceptibility of Hr-null MuSCs to mitotic catastrophe, we performed whole transcriptome RNA-seq analysis of quiescent MuSCs isolated from hindlimb muscles of Hr cKO and control mice (Fig. 4*C*). Using a 1% false-discovery rate, we identified 1,459 differentially expressed genes (DEGs) in MuSCs isolated from uninjured muscles of Hr cKO and control mice. Gene ontology term and pathway analysis of these genes using gene set enrichment analysis revealed that the term "cell cycle" was enriched with 123 DEGs (Fig. 4*D*). A large number of positive regulators of the cell cycle were down-regulated in Hr-null MuSCs (Fig. 4*E* and *SI Appendix*, Fig. S4*B*). Interestingly, the term "p53 signaling pathway" was also enriched in the DEGs (Fig. 4*D*), and in contrast to the down-regulation of cell cycle genes, genes involved in the p53 pathway were generally up-regulated in Hr-null MuSCs (Fig. 4*E* and *SI Appendix*, Fig. S4*C*). Proteins encoded by many of these genes implicated in the p53 pathway are enzymes involved in DNA repair, which include enzymes that can directly modify DNA molecules, such as the Apurinic/Apyrimidinic Endodeoxyribonuclease Apex2, the endonuclease Mus81 and the Tyrosyl-DNA phosphodiesterase Tdp2, and scaffold proteins that can recruit DNA-modifying enzymes to damage sites, such as Mdc1, Nabp1, Parp9, and Spidr. In addition, a number of genes encoding proteins that are known to delay or inhibit cell cycle progression in response to

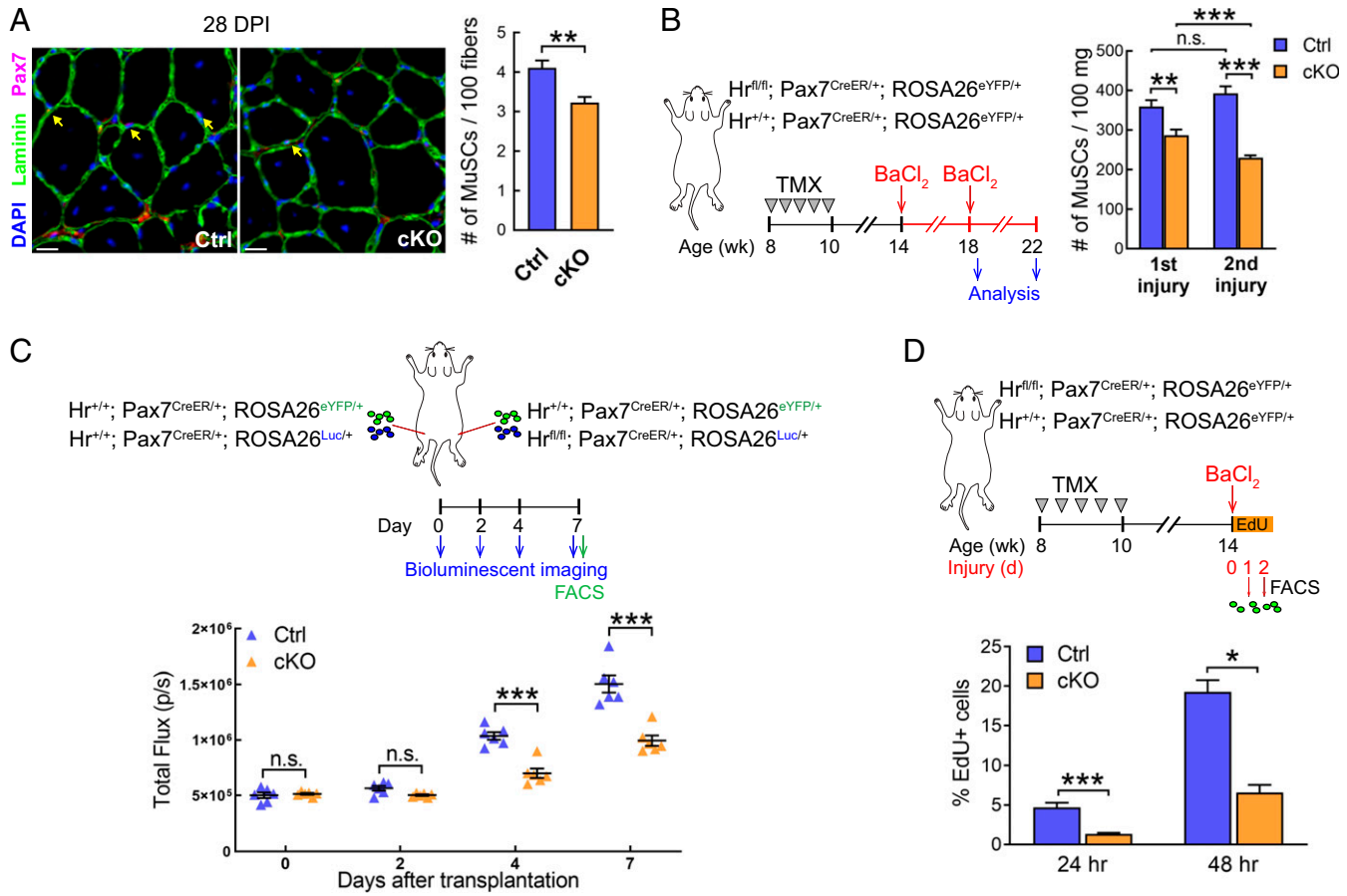

Fig. 3. Hr-null MuSCs are defective in self-renewal. (*A*) Representative images of TA cross-sections from Hr cKO and control mice 28 d after $BaCl_2$ injury and quantification of Pax7-expressing cells. (Scale bars, 10 μm.) (*B*) Quantification of MuSCs in Hr cKO and control mice after repeated injury. TA muscles of both legs of cKO or control animals ($n = 6$) were injured and allowed to recover for 4 wk, at which time one TA muscle of each animal was injured again. All TA muscles were harvested 4 wk after the second injury and weighed. The muscles were then dissociated for MuSC isolation and the numbers of YFP-expressing cells were quantified by FACS and normalized by the weight of the muscle. (*C*) Engraftment kinetics of Hr cKO and control MuSCs. The left TA muscle of each recipient mouse ($n = 6$) was injected with 5,000 freshly isolated YFP-expressing MuSCs from control mice mixed with 25,000 luciferase-expressing MuSCs from control mice. The right TA muscle of each recipient mice was injected with 5,000 YFP-expressing MuSCs from control mice mixed with 25,000 luciferase-expressing MuSCs from Hr cKO mice. The recipient mice were subjected to BLI immediately and then 2, 4, and 7 d after transplantation. The total flux of both TA muscles of each recipient mouse is plotted. (*D*) Delay in cell cycle entry of Hr-null MuSCs activated in vivo. Hr cKO or control mice ($n = 3$) were injured and fed with water containing EdU. MuSCs were isolated from these mice 1 or 2 d after injury. The percentage of EdU-incorporated cells in the total YFP^+ population was calculated. Data are shown as mean ± SEM; $^*P < 0.05$, $^{**}P < 0.01$, $^{***}P < 0.001$ (two-way ANOVA was performed for the reinjury experiment and Wilcoxon paired test was performed for the transplantation experiments).

DNA damaging agents—such as Mdc1, Npas2, Pttg1, and Fbxo6—were also found up-regulated in MuSCs from Hr cKO mice. These data suggest that lesions in genomic DNA may be present in Hr-null MuSCs, and that the delay in cell cycle entry of these cells may be consequent to the activation of checkpoint proteins.

Hr-Null MuSCs Are More Susceptible to Genotoxic Stress. We were interested in exploring how the function of Hr might relate to the phenotype of susceptibility to cell death and the transcriptome profile that suggests the presence of DNA damage and repair in Hr-null MuSCs. Hr shares domain homology with H3K9 demethylases Jmjd1a, Jmjd1b, and Jmjd1c in that they all contain a Zinc finger (ZF)-like domain and a Jumonji C domain (21). Given that di- and trimethylated H3K9 are features of heterochromatin, we hypothesized that loss of Hr may lead to alteration in heterochromatin structure. In order to directly assess whether chromatin structure is disrupted in Hr-null MuSCs, we performed electron microscopy (EM) and indeed found a significant decrease in heterochromatin content in MuSCs from Hr cKO compared to MuSCs from control mice (Fig. 5*A*). It has been shown that, in eukaryotic cells, compact heterochromatin structure is protective against genotoxic stress and that the loss of the compact structure renders the genome more susceptible to DNA damage (22, 23). In order to further test whether loss of heterochromatin in Hr-null MuSCs might lead to an increased susceptibility to genotoxic stress, we isolated MuSCs from cKO and control mice that had been subjected to different doses of irradiation and performed comet assays to quantify the extent of DNA damage in the cells. Consistent with previous findings (24), a lethal dose of irradiation led to the accumulation of DNA damage in over 80% of MuSCs in both control and cKO animals (Fig. 5*B*). However, lower doses of irradiation induced DNA damage in a significantly higher percentage of Hr cKO MuSCs in comparison to control cells (Fig. 5*B*). As a separate measure of DNA damage, we also quantified cells with γH2AX foci in MuSCs following irradiation and found that significantly more Hr cKO MuSCs exhibited γH2AX aggregates following low-dose irradiation (Fig. 5*C*). To ensure that the increased susceptibility of Hr cKO MuSCs to sublethal dose of irradiation was caused by intrinsic changes in these cells, we also subjected FACS-purified MuSCs to increasing doses of irradiation and found nearly 20%

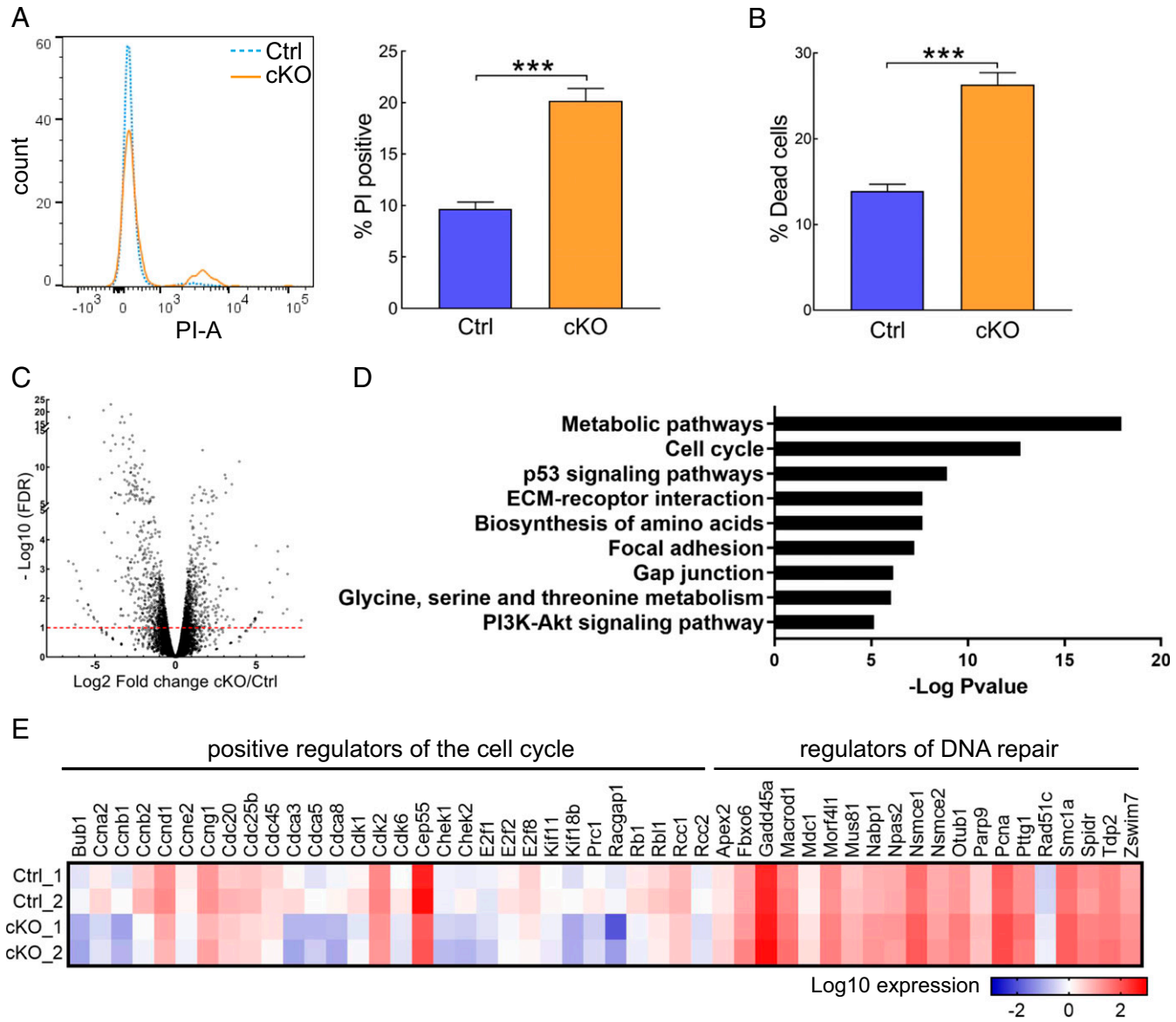

Fig. 4. Increased MuSC death upon activation in Hr cKO mice. (*A*) Quantification of dead cells in Hr cKO and control mice following muscle injury. MuSCs were isolated from Hr cKO or control mice 2.5 d after muscle injury and incubated with PI. The numbers of PI^+ cells were quantified by FACS. A representative FACS plot is shown on the left and the percentage of PI^+ cells (among total YFP^+ cells) from replicate studies ($n = 5$) is shown on the right. (*B*) Quantification of Hr-null MuSCs that die upon in vitro activation. MuSCs isolated from Hr cKO or control mice ($n = 5$) were plated and imaged by time-lapse microscopy. The number of cells that underwent cell death was recorded and the percentage of cells that died was calculated. (*C*) Volcano plot of the whole transcriptome by RNA-seq analysis of MuSCs isolated from Hr cKO and control mice. (*D*) Gene set enrichment analysis of hallmark gene sets and Kyoto Encyclopedia of Genes and Genomes (KEGG) pathways enriched in differentially expressed genes in MuSCs from Hr cKO and control mice. (*E*) Expression levels of cell cycle and DNA repair genes in MuSCs from Hr cKO and control mice. Data are shown as mean ± SEM in *A* and *B*; ***$P < 0.001$ (Welch's *t* tests).

more Hr cKO MuSCs exhibited DNA damage at low dose of irradiation (*SI Appendix*, Fig. S5 *A* and *B*). These studies clearly demonstrate that Hr-null MuSCs are more susceptible to DNA damage induced by genotoxic stress than control cells.

Mechanisms that protect cells from DNA damage have been shown to be important in maintaining a pool of functional stem cells during aging (25, 26). To determine whether Hr is important in protecting MuSCs from genotoxic stress during aging, we aged Hr cKO and control mice to 24 mo of age and performed comet assays to assess the level of DNA damage in these cells. With age, we indeed found a significant greater number of MuSCs exhibit DNA damage in cKO mice (Fig. 5*D*). We also quantified the number of MuSCs in TA muscles of 12- and 24-mo-old mice and found that the decline of MuSC numbers with age was greater in cKO compared to control mice (Fig. 5*E*). Taken together, these data demonstrate the importance of Hr in maintaining heterochromatin structure in MuSCs and protecting MuSCs from genotoxic stress.

Chromatin Architecture Is Altered in Hr-Null MuSCs. A hallmark of heterochromatin is H3K9me3. Given our observation that heterochromatin content decreases in Hr cKO MuSCs, we compared the levels of H3K9me2 and H3K9me3 in MuSCs from Hr cKO and control mice by Western blotting. We found a clear reduction in H3K9me3 in cKO MuSCs, whereas the level of H3K9me2 was unaffected (Fig. 6*A* and *SI Appendix*, Fig. S6 *A* and *B*). To directly assess the H3K9 methylation state in MuSCs, we performed chromatin immunoprecipitation-sequencing (ChIP-seq) analysis using MuSCs isolated from muscles of Hr cKO and control mice with antibodies

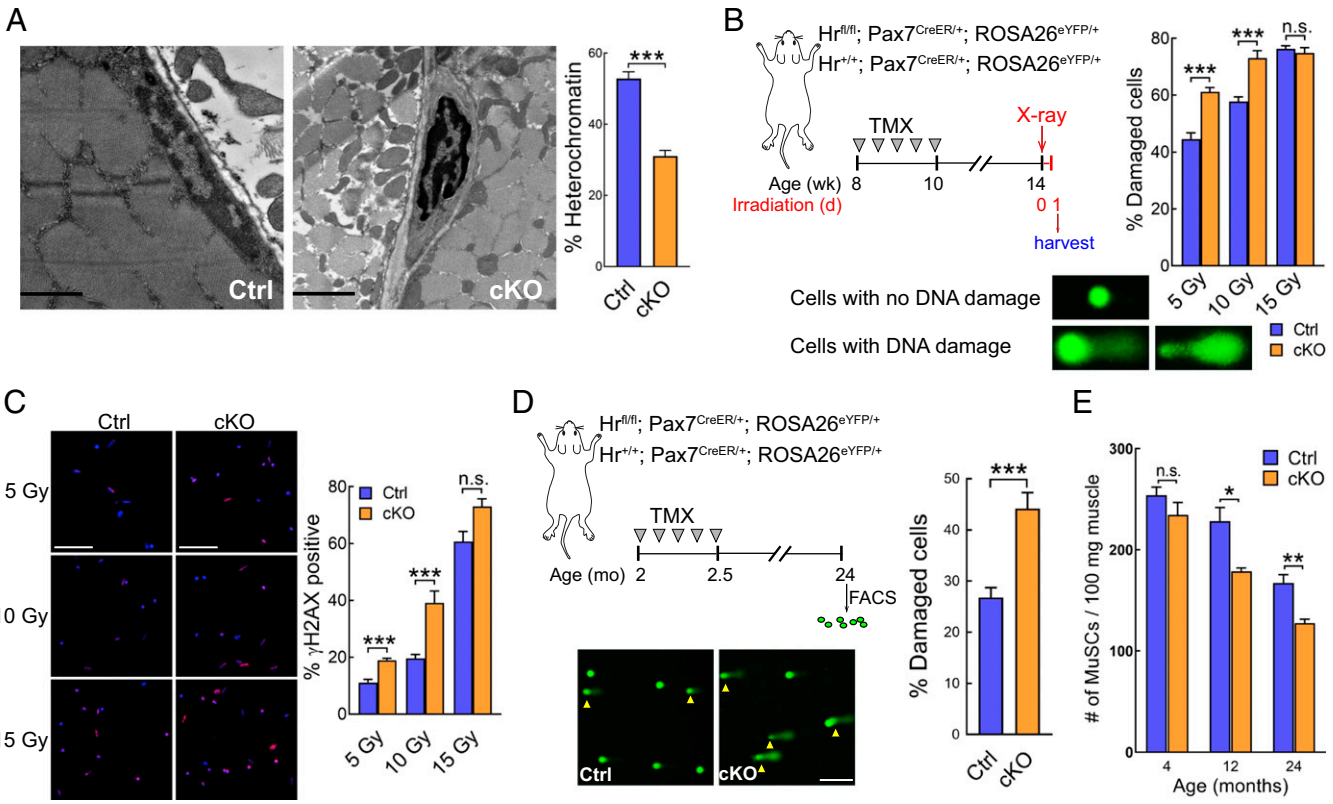

Fig. 5. Hr-null MuSCs exhibit changes in heterochromatin and are more susceptible to genotoxic stress. (*A*) EM analysis of Hr-null and control MuSCs ($n = 3$). Representative EM images of MuSCs from cKO and control mice are shown, *Left*. (Scale bars, 1 μm.) Quantification of heterochromatin content is shown on the right. The percentage of heterochromatin area over total area of the nucleus is plotted. (*B*) Increased susceptibility of Hr-null MuSCs to irradiation-induced DNA damage. The hindlimbs of Hr cKO or control mice ($n = 4$) were subjected to 5, 10, or 15 Gy γ-irradiation. MuSCs were isolated from the hindlimb muscles 1 d after irradiation and immediately analyzed by alkaline comet assay. The numbers of cells with or without DNA damage were then quantified. (*Upper Left*) Schematic of the experimental setup and time line. (*Lower Left*) Representative images of cells after electrophoresis. (*Right*) Graph illustrating the percentages of cells exhibiting DNA damage in response to each dose of irradiation. (*C*) γH2AX immunofluorescence images and quantification of MuSCs after irradiation. MuSCs isolated from irradiated Hr cKO or control mice as described in *B* were plated and stained with antibodies specific to phosphorylated H2AX. Representative images are shown, *Left*, and the percentages of $\gamma H2AX^+$ MuSCs (i.e., YFP-expressing cells) are shown, *Right*. (Scale bars, 50 μm.) (*D*) Quantification of cells with DNA damage in Hr-null MuSCs with age. MuSCs isolated from 24-mo-old Hr cKO or control mice ($n = 6$) were analyzed by alkaline comet assay. Representative images are shown, *Lower Left*. (Scale bars, 50 μm.) The percentages of cells exhibiting damaged DNA in the total MuSC population are shown on the right. (*E*) Quantification of the number of MuSCs in the TA muscles of Hr cKO and control mice during aging. TA muscles were harvested from 4-, 12-, and 24-mo-old Hr cKO or control mice ($n = 6$) and weighed. The numbers of YFP-expressing MuSCs were quantified by FACS. The numbers of MuSCs normalized to the weights of the TA muscles are plotted. Data are shown as mean ± SEM; $^*P < 0.05$, $^{**}P < 0.01$, $^{***}P < 0.001$ (unpaired *t* tests).

specific to H3K9me3. Nearly 60% of H3K9me3 peaks were found in distal intergenic regions (Fig. 6*B* and *SI Appendix*, Fig. S6*C*). Across the gene body, H3K9me3 peaks were found predominantly within introns. When we visualized the H3K9me3 ChIP-seq profiles, we found that a number of genes exhibited loss of H3K9me3 peaks at their transcription start sites (TSSs) and a reduction of overall coverage throughout the gene body (Fig. 6*C*). We then performed metagene analysis to compare the densities of H3K9me3 reads both in the gene body and in downstream and upstream flanking regions across the genome. The density of H3K9me3 exhibited a decrease in both the gene body and up to 10-kb downstream and upstream of the genes in Hr cKO MuSCs (Fig. 6*D*). As such changes of H3K9me3 levels around TSSs did not appear to associate with changes in transcription (*SI Appendix*, Fig. S6*D*), these ChIP-seq analyses reveal a global reduction of H3K9me3 in Hr cKO MuSCs that is likely independent of transcription status.

Due to the association of H3K9me3 with compact chromatin, we then hypothesized that a global reduction of H3K9me3 is accompanied by an increase in open chromatin. To test this hypothesis, we performed assay for transposase accessible chromatin using sequencing (ATAC-seq) on MuSCs isolated from Hr cKO and control mice. We first performed insert size analysis to confirm that the sequenced fragments from MuSCs exhibited periodicity of ~200 bp, as expected from ATAC-seq libraries (*SI Appendix*, Fig. S6*E*), and Pearson correlation to reveal difference in cKO and control MuSCs (*SI Appendix*, Fig. S6*F*). We then calculated the read density 2 kb around TSSs across the genome and found that not only did the read intensity increase in regions immediately around TSSs, but also the regions with high read density spread further away from TSSs (*SI Appendix*, Fig. S6*G*). We also calculated the read density at CpG islands, which are usually located at the promoters of housekeeping genes and found higher read density in Hr cKO MuSCs (*SI Appendix*, Fig. S6*H*). Taken together, the ChIP-seq and ATAC-seq analyses revealed that Hr maintains proper H3K9me3 in MuSCs. Loss of Hr leads to a reduction in H3K9me3 and an increase in open chromatin around TSSs and gene-regulatory regions.

Hr Regulates H3K9 Demethylase Activity. Because Hr contains a Jumonji domain that is conserved among the Jumonji superfamily of histone demethylases and shares protein domain homology with H3K9 demethylases Jmjd1a, Jmjd1b, and Jmjd1c, it has been proposed to be an H3K9 demethylase itself. However, the reduction of H3K9me3 in Hr-null cells is at odds with the notion

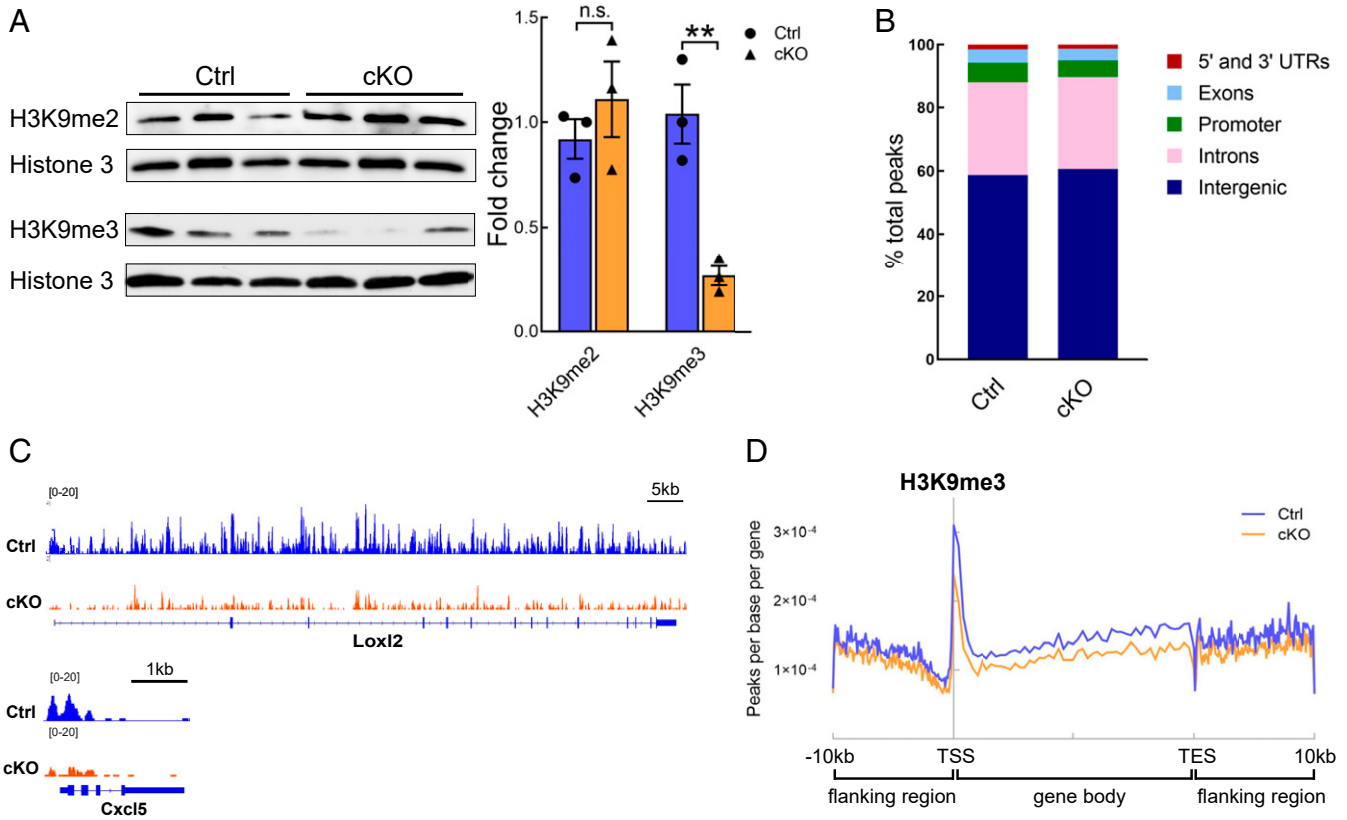

Fig. 6. Heterochromatin architecture is disrupted in Hr-null MuSCs. (*A*) Western blot analysis of H3K9me2 and H3K9me3 levels in MuSCs from Hr cKO and control mice. MuSCs were isolated from Hr cKO or control mice ($n = 3$). Total protein extracted from 10^5 cells from each mouse was analyzed by SDS/PAGE followed by Western blotting with an antibody specific to H3K9me2 or H3K9me3. Blots were then reprobed with a pan-Histone 3 antibody. A representative Western blot is shown, *Left*. To quantify H3K9me2 and H3K9me3 levels, the relative density of H3K9me3 bands was normalized to the relative density of pan-Histone 3 bands. The normalized H3K9me2 and H3K9me3 levels in cKO in comparison to control cells is plotted, *Right*. (*B*) Fraction of H3K9me3 peaks associated with different genomic features in control (Ctrl) and Hr cKO MuSCs. (*C*) Examples of H3K9me3 tracks showing reduction in cKO MuSCs at both the TSSs and gene body. (*D*) Metagene analysis of H3K9me3 distribution at gene bodies and 10-kb upstream and downstream flanking regions. TSS: transcription start site. TES: transcription end site. Data are shown as mean ± SEM in *A*; **$0.001 < P < 0.01$ (unpaired *t* tests).

that Hr functions as a H3K9 demethylase. We therefore set out to determine the mechanism by which Hr regulates cellular H3K9 methylation levels. First, we sought to determine the effect of Hr expression on H3K9 methylation levels in cells that do not normally express the gene. Unlike Jmjd1a, whose overexpression led to a reduction in mono- and dimethylation of H3K9 (Fig. 7*A*), or Jmjd2a, whose overexpression led to a reduction in trimethylation of H3K9 (*SI Appendix*, Fig. S7*A*), overexpression of Hr not only did not decrease any form of methylated H3K9, but also resulted in a slight increase in H3K9me1 and H3K9me2 (Fig. 7*A*) and a significant increase in H3K9me3 (Fig. 7*B* and *SI Appendix*, Fig. S7 *A* and *B*). Interestingly, we found that, knockout of Jmjd1a expression led to an increase in H3K9me3 but not H3K9me2 (*SI Appendix*, Fig. S7*C*), demonstrating that inhibition of Jmjd1a activity leads secondarily to an increase in H3K9me3 levels. We then performed a cell-free demethylase assay in which purified methylated H3K9 peptides were incubated with Hr protein in the presence of cofactors that are required for Jumonji-containing demethylases. This assay confirmed that Hr lacks the activity to demethylate H3K9me2 or H3K9me3 (Fig. 7*C*). As the lack of demethylase activity of Hr could be due to its inability to recognize methylated H3K9, we then performed an in vitro binding assay using purified Hr proteins and H3 peptides methylated at various lysines. Using this assay, we consistently detected interaction between Hr and di- and trimethylated H3K9 (Fig. 7*D*). We also generated various truncated forms of Hr (*SI Appendix*, Fig. S7*D*) and found that both the ZF-like and JmjC domains were capable of binding to di- and trimethylated H3K9 peptides (*SI Appendix*, Fig. S7*E*).

Given that Hr is capable of binding to methylated H3K9 peptides but lacks demethylase activity, we hypothesized that the binding of methylated H3K9 by Hr may prevent other demethylases from recognizing their substrate. To test this hypothesis, we determined the effect of Hr expression on the activities of the H3K9me2 demethylase Jmjd1a and the H3K9me3 demethylase Jmjd2a. We found that, in the presence of increasing amount of Hr, the ability of Jmjd1a to demethylate H3K9me2 was progressively inhibited (Fig. 7*E*). This result was confirmed using a cell-free demethylase assay in which purified dimethylated H3K9 peptides were incubated with the demethylase Jmjd1a in the presence of varying amounts of Hr protein (*SI Appendix*, Fig. S7*F*). However, despite the fact that loss of Hr in MuSCs is associated with a lower level of H3K9me3, Hr does not appear to directly inhibit Jmjd2a, as we found that the expression of Hr had a negligible effect on the ability of Jmjd2a to demethylate H3K9me3 even at the highest dose (*SI Appendix*, Fig. S7 *A*, *B*, and *G*). We have also performed co-IP assays to confirm that Hr expression does not abolish the interaction between heterochromatin protein 1α (HP1α) and H3K9me2/3 (*SI Appendix*, Fig. S7*H*). These data demonstrate that Hr is a regulator of H3K9 demethylation rather than acting as a demethylase itself.

The ability of Hr to maintain heterochromatin and prevent genotoxic stress in MuSCs is based on its ability to bind to H3K9me2/3 and act as an inhibitor of demethylase activity at

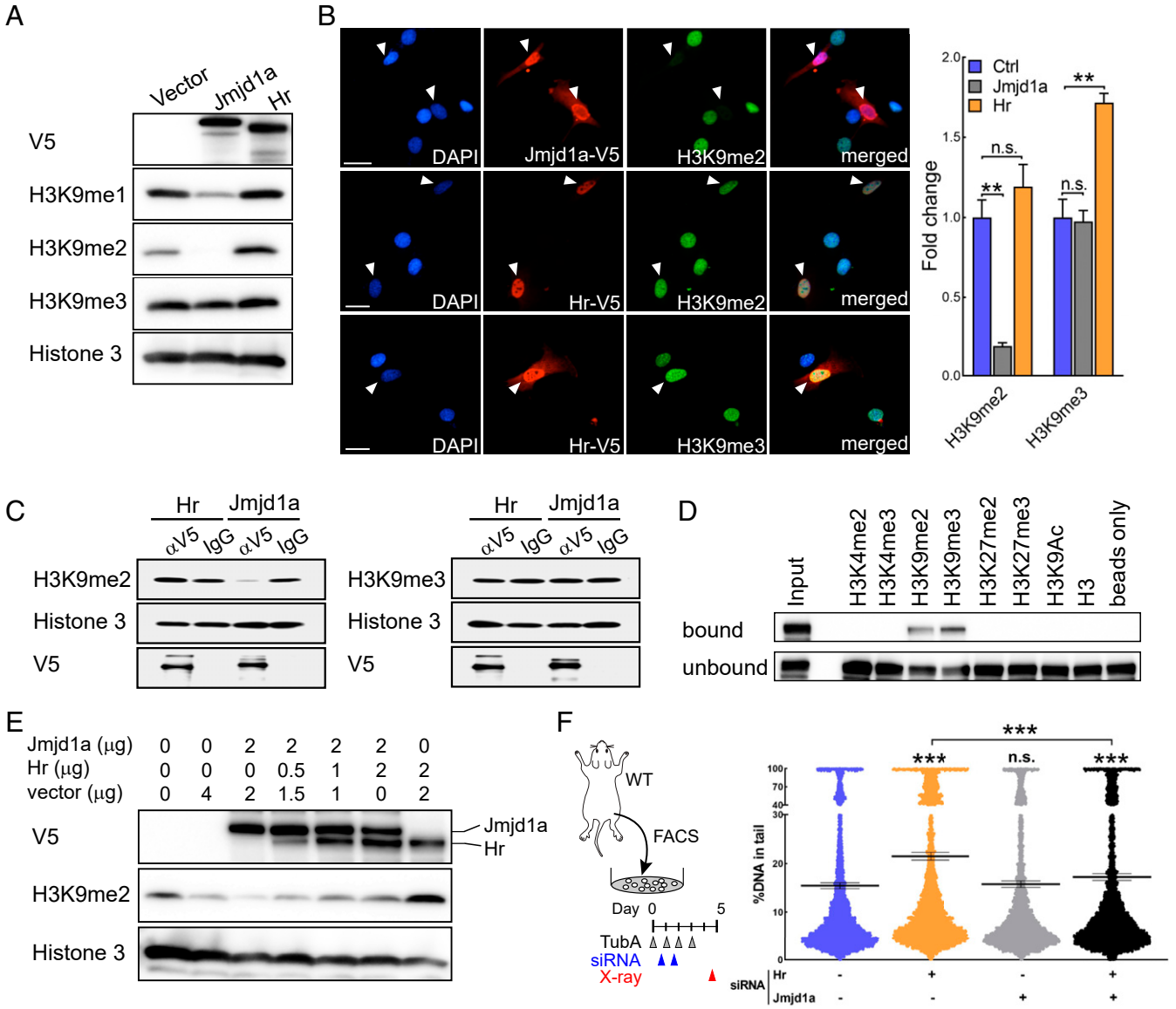

Fig. 7. Hr regulates H3K9 demethylase activity. (*A*) Western blot analysis of mono-, di-, and trimethylation of H3K9 upon overexpression of Jmjd1a or Hr in 293T HEK cells. 293T cells were transfected with plasmid vector control or plasmids encoding V5 epitope-tagged Jmjd1a or Hr. Total protein was extracted from cells 48 h after transfection and analyzed by SDS/PAGE followed by Western blotting with antibodies specific to mono- (H3K9me1), di- (H3K9me2), and tri- (H3K9me3) methylated Histone 3 Lysine 9. Blots were reprobed with a pan-Histone 3 antibody. The expression of Jmjd1a and Hr was assessed using an antibody specific to the V5 epitope. (*B*) Immunofluorescent images of cells expressing Hr. C2C12 cells were transfected with a plasmid to expressed Jmjd1a-V5 or Hr-V5. Cells were fixed 48 h after transfection and stained with anti-V5 and with anti-H3K9me2 or anti-H3K9me3 antibodies. (Scale bars, 5 μm.) Cells expressing Hr-V5 are indicated by arrowheads. The intensity of H3K9me2 and H3K9me3 was quantified. The fold change between cells expressing Jmjd1a-V5 or Hr-V5 and untransfected in the vicinity was calculated and plotted, *Right*. (*C*) Cell-free demethylase assay of Jmjd1a and Hr. Histone 3 proteins were incubated with purified Hr or Jmjd1a in the presence of cofactors necessary for demethylase activity. The methylation levels were analyzed by Western blotting using antibodies specific to H3K9me2 and H3K9me3. (*D*) In vitro binding assay of Hr and purified methylated Histone 3 peptides. Equal amounts of Histone 3 peptides containing the indicated modification were immobilized on Streptavidin beads and incubated with lysate prepared from 293T cells expressing V5-tagged Hr proteins. Both the fraction of proteins bound to the beads and unbound fraction were analyzed by SDS/PAGE followed by Western blotting with a V5 antibody. (*E*) Coexpression of Hr with Jmjd1a inhibits the demethylase activity of Jmjd1a. 293T cells were transfected with fixed amount of Jmjd1a-V5 plasmid and increasing amount of Hr-V5 plasmid. Lysates were prepared from cells 72 h after transfection and analyzed by SDS/PAGE followed by Western blotting with antibodies specific to H3K9me2 and pan-Histone 3. The expression levels of Jmjd1a and Hr were assessed with the V5 antibody. (*F*) Jmjd1a silencing ameliorates the increased susceptibility of MuSCs to low-dose irradiation in the absence of Hr. MuSCs were isolated from wild-type mice by FACS and treated with 40 μM Tubastatin A (Tub A) for 4 d. On the first and second days after isolation, cells were transfected with siRNAs targeting Hr, Jmjd1a, or both. Cells were then exposed to 100-mGy irradiation and DNA damage of the irradiated cells was assessed by comet assay. Images were analyzed by the ImageJ add-on package OpenComet (53) to obtain the percentage of DNA that is in the comet tail of each cell. Statistics were calculated for the comparisons between each RNAi condition and the control, and between the Hr and Jmjd1a double knockdown and Hr knockdown conditions. Data are shown as mean ± 95% CI. $*P < 0.05$, $**P < 0.01$, $***P < 0.001$ (unpaired *t* tests).

these specific histone modifications. We therefore tested the hypothesis that inhibiting the activity of Jmjd1a would ameliorate the increased susceptibility of MuSCs to genotoxic stress due to the loss of Hr. Because Hr expression rapidly decreases with MuSC activation, we isolated MuSCs from wild-type mice and maintained them in a culture condition that prevents them from entering the cell cycle (11). We confirmed that culturing MuSCs in this condition maintains the expression of Hr and has no impact on the expression of Jmjd1a (*SI Appendix*, Fig. S7*I*). We then transfected these cells with siRNAs specific to Hr and Jmjd1a prior to exposing them to low dose irradiation. Consistent with our previous finding that MuSCs from Hr cKO mice exhibit increased susceptibility to irradiation, knockdown of Hr led to an increase in the level of DNA damage (Fig. 7*F* and *SI Appendix*, Fig. S7*J*). While knockdown of Jmjd1a alone did not affect the susceptibility of these cells to irradiation, we observed lower levels of DNA damage in cells in which both Hr and Jmjd1a are knocked down. Taken together, these data indicate that Hr maintains heterochromatin integrity by antagonizing Jmjd1a in MuSCs.

Discussion

Molecular Function of Hr. The first mammalian *Hr* gene was discovered by cloning the retroviral insertion site in the *Hr* allele of the naturally occurring hairless house mice (27). Much of the early molecular characterization of the Hr protein focused on understanding its regulation by nuclear receptors (16, 28–30). In light of the discovery of the superfamily of Jumonji domain-containing histone demethylases, Hr was found to contain a JmjC domain at the carboxyl terminus and to share domain similarity with mono- and dimethyl-H3K9 demethylases Jmjd1a, Jmjd1b, and Jmjd1c (21). Although the JmjC domain of Hr lacks all but one cofactor binding site, it was reported to be an H3K9 demethylase since a partial Hr protein that contained the JmjC domain but lacked the amino (N) terminus was able to reduce slightly the level of monomethyl-H3K9 when incubated with histone proteins in vitro (31). In contrast, when we performed similar in vitro demethylase assays with full-length Hr and purified histone proteins, we did not detect enzymatic activity in Hr despite the fact that it can bind directly to di- and trimethylated H3K9 peptides. The N terminus of Hr clearly lacks binding capacity to methylated H3K9 (*SI Appendix*, Fig. S7*E*). However, the deletion of the N terminus enhances the interaction between methylated H3K9 and Hr (*SI Appendix*, Fig. S7*E*). This suggests that the N terminus of Hr plays a regulatory role that is required for normal Hr function, and that the activity of a partial Hr protein lacking the N terminus is likely to be dysregulated. A recent publication suggested that Hr is a substrate of protein kinase C and identified putative phosphorylation sites that localize within the N-terminal domain (32). Whether phosphorylation at these sites regulates the interaction of Hr with methylated H3K9 and its function of the Hr protein requires further investigation.

Our studies suggest that Hr functions as an H3K9 demethylase antagonist. Hr binds to H3K9me2 and H3K9me3 and prevents them from being recognized by specific demethylases, thus regulating H3K9 methylation. We found that overexpression of Hr inhibits the demethylase activity of H3K9me2 demethylase Jmjd1a but not H3K9me3 demethylase Jmjd2a. However, we did not detect a change in the H3K9me2 levels either in cells overexpressing Hr or in Hr-null MuSCs. Rather, overexpression of Hr leads to an increase in H3K9me3, and Hr ablation leads to a decrease in H3K9me3 in MuSCs. This is likely attributable to a shift in the overall steady-state balance between methyltransferase and demethylase activity once a regulatory mechanism is disrupted. As such, changes in the activity of Jmjd1a can have an indirect effect on the level of H3K9me3. Consistent with this model, we found that the knockdown of Jmjd1a had a negligent effect on the H3K9me2 levels but led to an increase in the levels of H3K9me3 in myogenic cells (*SI Appendix*, Fig. S7*C*). This is a demonstration that a histone demethylase can be inhibited by an enzymatically dead member of the same family. Further studies are required to determine whether Hr has demethylase activity on nonhistone substrates.

Hr Expression and Function in Stem Cells. Interestingly, both loss-of-function and gain-of-function mutations in the *Hr* gene cause congenital hair disorders in human. Mutations that inactivate Hr cause congenital atrichia with papular lesions (APL, OMIM #209500), an autosomal recessive form of total alopecia (33, 34). Individuals affected by APL are born with normal hair patterns. However, their hair is usually shed within months after birth and never replaced, consistent with the phenotype of all mouse strains bearing various forms of germline deletions or mutations of the Hr gene (35). All these mice, as well as the Hr cKO mice we generated and used in this study, exhibit no developmental defect despite obvious defects in hair and muscle regeneration. In contrast, some cases of Marie Unna hereditary hypotrichosis (MUHH, OMIM # 146550), a rare inheritable hair loss disorder associated with increased translation of the Hr protein (36), exhibit limb deformities (37). Whether gain-of-function mutations of the *Hr* gene affect skeletal muscle development will require further investigation.

In mouse, Hr expression was found as early as embryonic day12.5 in nervous tissues, in cartilage, and in the epithelium of a large number of tissues and organs with the exception of testes, liver, heart, and kidney (38). In adult animals, robust Hr expression is found only in skin and brain at the tissue level (38). In skin, the expression of Hr in follicles oscillates during the hair cycle (39). Despite this link between Hr expression and the quiescent phase of skin stem cells, a direct link between Hr and stem cell function has not been established. Hr expression has not previously been reported in skeletal muscle at the tissue level in adult animals. We and others have found Hr is one of the most down-regulated genes when MuSCs are activated ex vivo (12, 40). Here we have demonstrated the presence of both Hr mRNA and protein in quiescent MuSCs. As in the hair cycle, the expression of Hr also oscillates during muscle regeneration. Upon muscle injury, Hr expression is rapidly and drastically down-regulated during the early phase of regeneration when MuSCs are activated. Hr expression is undetectable in proliferating myoblasts and reestablished when self-renewed MuSCs re-enter quiescence. In addition, our study directly demonstrates the important role of Hr in maintaining H3K9me3 and heterochromatin integrity in adult MuSCs.

Genome Integrity and Stem Cell Aging. Loss of heterochromatin has been proposed as a model of cellular aging based on findings that a gain-of-function mutation of the yeast heterochromatin promoting protein Sir4 extends yeast life span by 30%, and aging yeast exhibit a loss in heterochromatin-mediated silencing (41–43). A gradual loss of heterochromatin has been correlated with age in other eukaryotic species, including worms, flies, and humans (44–47). It has recently been shown that H3K9me3-marked heterochromatin regulates nuclear stiffness to prevent DNA damage resulting from mechanical forces (48). Quiescent MuSCs were identified by their significantly higher levels of heterochromatin in comparison to myonuclei (1, 3). It was previously reported that although ablation of the methyltransferase Ehmt2/G9a in myogenic progenitors leads to disruption of H3K9me2, muscle development or regeneration appears grossly normal (49). However, it is unclear whether the heterochromatin integrity is compromised in the MuSCs from these knockout animals. Our finding that Hr cKO MuSCs, which exhibit a loss in H3K9me3-marked heterochromatin, are more susceptible to genotoxic stress highlights the protective role of heterochromatin against the accumulation of DNA damage. We recently identified both Hr and Jmjd1a as genes that exhibit reduced levels of expression in MuSCs from aged animals, with the reduction in Hr expression more prominent

than that in Jmjd1a (11). In this study, in comparison to control animals of the same age, 2-y-old Hr cKO mice have reduced number of MuSCs and exhibit more extensive DNA damage in the remaining pool of MuSCs. The Hr-Jmjd1a antagonism is likely to have a role in safeguarding MuSC function during aging and a deficiency of this protective process increases the susceptibility of MuSCs to genotoxic stress and leads to an acceleration of age-related decline in MuSC numbers. As loss of Hr expression is associated with a reduction in H3K9me3 levels and heterochromatin content, these findings attest to the importance of heterochromatin maintenance in stem cell homeostasis and function. As such, our studies provide a direct link bridging the loss of heterochromatin model of aging and the DNA damage model of aging.

It is worth noting that Hr deficiency in young MuSCs does not lead to stem cell depletion but rather to functional impairments that resemble those of aged MuSCs (20). In early studies with adult Hr germline mutant mice, morphological abnormalities were observed in a number of tissues (38). For example, the thickness of the inner plexiform and ganglion cell layers in retina is reduced in comparison to age-matched controls, hyperproliferation of the epithelium, and increased number of villi is found in the colon and the thymus exhibits significant atrophy. In addition, Hr mutant mice older than 1 y of age show severe hearing loss, and histological analysis revealed a degeneration of the cochlear sensory epithelium and reduced number of neurons in the inner ear (38). All of these phenotypes resemble typical changes found in these tissues and organs of old animals. Although Hr expression was below the level of detection in total cellular extracts from these tissues in young animals, it will be interesting to determine whether the gene is expressed in rare quiescent stem or progenitor cells residing in these tissues and whether it functions in those cells in ways analogous to what we have described in MuSCs. Such studies will test whether Hr is a guardian of the genome against genotoxic stress and aging in quiescent stem cells more generally.

Experimental Procedures

Animals. $Hr^{flox/flox}$ mice were generated by GenOway. $Pax7^{tm1(cre/Esr1*)Cklr}$ ($Pax7^{CreER/CreER}$) and $Gt(ROSA)26Sor^{tm1.1(CMV\text{-}Luc,\ \text{-}ALPP)Cklr}$ ($Rosa26^{LUSEAPm}$) mice were gifts from Charles Keller, Oregon Health & Science University, Portland, OR (18). B6.129 × 1-$GT(ROSA)26Sor^{tm1(EYFP)Cos}$/J ($Rosa26^{eYFP/eYFP}$) and Tg(KRT14-cre/ERT)20Efu/J ($K14\text{-}CreER^{tam}$) were purchased from Jackson Laboratory. All animals used in this study were housed and maintained in the Veterinary Medical Unit at the Veterans Affairs Palo Alto Health Care System. Animal protocols were approved by the Institutional Animal Care and Use Committee. Unless stated otherwise, 3- to 5-mo-old mice were used in the experiments.

MuSC Isolation and Treatment. Isolation of skeletal MuSCs by sequential enzymatic digest followed by FACS was performed as previously described (50). Sorted MuSCs were routinely analyzed by FACS immediately after sorting and by immunofluorescence with Pax7 antibody to ensure high purity.

Next-Generation Sequencing. For RNA-seq, RNA was extracted from MuSCs using the RNeasy Micro Plus Kit (Qiagen) according to the manufacturer's instructions. Reverse transcription was performed using the SMART-Seq v4 Ultra Low Input RNA Kit (Takara) according to manufacturer's instructions. The cDNA was then sheared with a Covaris ultrasonicator and library constructions were performed with the Ovation Ultralow Multiplex system (NuGEN). For ChIP-seq, MuSCs were incubated with 1% formaldehyde as previously described (12, 20) and stored at −80 °C until lysis. Chromatin fragmentation was performed in a Covaris ultrasonicator. ChIP was performed with the Magnify Chromatin Immunoprecipitation System (Invitrogen) according to the manufacturer's instructions. Library constructions were performed with the Ovation Ultralow Multiplex system (NuGEN). ATAC-seq libraries were generated according to previously published protocols (51, 52). All libraries were sequenced in a HiSEq. 4000 sequencer (Illumina) at the Stanford Genome Sequencing Service Center.

Statistical Analysis. All statistical analyses were performed using GraphPad Prism 8 (GraphPad Software). Significance was calculated using two-tailed, unpaired Student's *t* tests unless stated otherwise. Differences were considered to be statistically significant at the $P < 0.05$ level (*$P < 0.05$, **$P < 0.01$, ***$P < 0.001$, ns: not significant).

Data Availability. The data reported in this paper have been deposited in the Gene Expression Omnibus (GEO) database (accession no. GSE132256).

ACKNOWLEDGMENTS. We thank all members of the T.A.R. laboratory for helpful discussions; Dr. Charles Keller for generously providing reagents; Yuzhen Wang and Heather Ishak for assistance with mouse husbandry; Samantha Thomson for histology processing; John Perrino at Stanford Cell Sciences Imaging Facility for assistance with electron microscopy; Corey Cain and Brandon Carter for assistance at the Palo Alto Veterans Institute for Research FACS core; and the Stanford Genome Technology Center for assistance with high-throughput sequencing. This work was supported by the Glenn Foundation for Medical Research, and by grants from the Department of Veterans Affairs (BLR&D and RR&D Merit Reviews) and the NIH (P01 AG036695, R37 AG023806, R01 AR073248, and TR01 AG047820) to T.A.R.

1. A. Mauro, Satellite cell of skeletal muscle fibers. *J. Biophys. Biochem. Cytol.* **9**, 493–495 (1961).
2. P. S. Zammit *et al.*, Pax7 and myogenic progression in skeletal muscle satellite cells. *J. Cell Sci.* **119**, 1824–1832 (2006).
3. V. Boonsanay *et al.*, Regulation of skeletal muscle stem cell quiescence by Suv4-20h1-dependent facultative heterochromatin formation. *Cell Stem Cell* **18**, 229–242 (2016).
4. A. Loyola, T. Bonaldi, D. Roche, A. Imhof, G. Almouzni, PTMs on H3 variants before chromatin assembly potentiate their final epigenetic state. *Mol. Cell* **24**, 309–316 (2006).
5. A. H. Peters *et al.*, Partitioning and plasticity of repressive histone methylation states in mammalian chromatin. *Mol. Cell* **12**, 1577–1589 (2003).
6. J. C. Peng, G. H. Karpen, Heterochromatic genome stability requires regulators of histone H3 K9 methylation. *PLoS Genet.* **5**, e1000435 (2009).
7. Y. Sun *et al.*, Histone H3 methylation links DNA damage detection to activation of the tumour suppressor Tip60. *Nat. Cell Biol.* **11**, 1376–1382 (2009).
8. C. Höög, M. Schalling, E. Grunder-Brundell, B. Daneholt, Analysis of a murine male germ cell-specific transcript that encodes a putative zinc finger protein. *Mol. Reprod. Dev.* **30**, 173–181 (1991).
9. K. Yamane *et al.*, JHDM2A, a JmjC-containing H3K9 demethylase, facilitates transcription activation by androgen receptor. *Cell* **125**, 483–495 (2006).
10. Y. H. Loh, W. Zhang, X. Chen, J. George, H. H. Ng, Jmjd1a and Jmjd2c histone H3 Lys 9 demethylases regulate self-renewal in embryonic stem cells. *Genes Dev.* **21**, 2545–2557 (2007).
11. J. O. Brett *et al.*, Exercise rejuvenates quiescent skeletal muscle stem cells in old mice through restoration of Cyclin D1. *Nat. Metab.* **2**, 307–317 (2020).
12. L. Liu *et al.*, Chromatin modifications as determinants of muscle stem cell quiescence and chronological aging. *Cell Rep.* **4**, 189–204 (2013).
13. J. K. Parrish, M. Sechler, R. A. Winn, P. Jedlicka, The histone demethylase KDM3A is a microRNA-22-regulated tumor promoter in Ewing sarcoma. *Oncogene* **34**, 257–262 (2015).
14. M. B. Cheng *et al.*, Specific phosphorylation of histone demethylase KDM3A determines target gene expression in response to heat shock. *PLoS Biol.* **12**, e1002026 (2014).
15. T. Kouzarides, Chromatin modifications and their function. *Cell* **128**, 693–705 (2007).
16. G. B. Potter *et al.*, The hairless gene mutated in congenital hair loss disorders encodes a novel nuclear receptor corepressor. *Genes Dev.* **15**, 2687–2701 (2001).
17. V. Vasioukhin, L. Degenstein, B. Wise, E. Fuchs, The magical touch: Genome targeting in epidermal stem cells induced by tamoxifen application to mouse skin. *Proc. Natl. Acad. Sci. U.S.A.* **96**, 8551–8556 (1999).
18. K. Nishijo *et al.*, Biomarker system for studying muscle, stem cells, and cancer in vivo. *FASEB J.* **23**, 2681–2690 (2009).
19. S. Srinivas *et al.*, Cre reporter strains produced by targeted insertion of EYFP and ECFP into the ROSA26 locus. *BMC Dev. Biol.* **1**, 4 (2001).
20. L. Liu *et al.*, Impaired notch signaling leads to a decrease in p53 activity and mitotic catastrophe in aged muscle stem cells. *Cell Stem Cell* **23**, 544–556.e4 (2018).
21. R. J. Klose, E. M. Kallin, Y. Zhang, JmjC-domain-containing proteins and histone demethylation. *Nat. Rev. Genet.* **7**, 715–727 (2006).
22. R. J. O'Sullivan, S. Kubicek, S. L. Schreiber, J. Karlseder, Reduced histone biosynthesis and chromatin changes arising from a damage signal at telomeres. *Nat. Struct. Mol. Biol.* **17**, 1218–1225 (2010).
23. D. Liang, S. L. Burkhart, R. K. Singh, M. H. Kabbaj, A. Gunjan, Histone dosage regulates DNA damage sensitivity in a checkpoint-independent manner by the homologous recombination pathway. *Nucleic Acids Res.* **40**, 9604–9620 (2012).
24. A. Scaramozza *et al.*, Lineage tracing reveals a subset of reserve muscle stem cells capable of clonal expansion under stress. *Cell Stem Cell* **24**, 944–957.e5 (2019).
25. D. J. Rossi *et al.*, Deficiencies in DNA damage repair limit the function of haematopoietic stem cells with age. *Nature* **447**, 725–729 (2007).
26. A. Nijnik *et al.*, DNA repair is limiting for haematopoietic stem cells during ageing. *Nature* **447**, 686–690 (2007).
27. J. P. Stoye, S. Fenner, G. E. Greenoak, C. Moran, J. M. Coffin, Role of endogenous retroviruses as mutagens: The hairless mutation of mice. *Cell* **54**, 383–391 (1988).

28. C. C. Thompson, M. C. Bottcher, The product of a thyroid hormone-responsive gene interacts with thyroid hormone receptors. *Proc. Natl. Acad. Sci. U.S.A.* **94**, 8527–8532 (1997).
29. J. C. Hsieh *et al*., Physical and functional interaction between the vitamin D receptor and hairless corepressor, two proteins required for hair cycling. *J. Biol. Chem.* **278**, 38665–38674 (2003).
30. A. N. Moraitis, V. Giguère, C. C. Thompson, Novel mechanism of nuclear receptor corepressor interaction dictated by activation function 2 helix determinants. *Mol. Cell. Biol.* **22**, 6831–6841 (2002).
31. L. Liu *et al*., Hairless is a histone H3K9 demethylase. *FASEB J.* **28**, 1534–1542 (2014).
32. L. Brook, G. K. Whitfield, D. Hsieh, R. D. Bither, J. C. Hsieh, The mammalian hairless protein as a DNA binding phosphoprotein. *J. Cell. Biochem.* **118**, 341–350 (2017).
33. W. Ahmad *et al*., Alopecia universalis associated with a mutation in the human hairless gene. *Science* **279**, 720–724 (1998).
34. A. Zlotogorski, A. A. Panteleyev, V. M. Aita, A. M. Christiano, Clinical and molecular diagnostic criteria of congenital atrichia with papular lesions. *J. Invest. Dermatol.* **118**, 887–890 (2002).
35. C. C. Thompson, Hairless is a nuclear receptor corepressor essential for skin function. *Nucl. Recept. Signal.* **7**, e010 (2009).
36. Y. Wen *et al*., Loss-of-function mutations of an inhibitory upstream ORF in the human hairless transcript cause Marie Unna hereditary hypotrichosis. *Nat. Genet.* **41**, 228–233 (2009).
37. K. Farkas, N. Nagy, A. Kinyó, L. Kemény, M. Széll, A newly identified missense mutation of the HR gene is associated with a novel, unusual phenotype of Marie Unna hereditary hypotrichosis 1 including limb deformities. *Arch. Dermatol. Res.* **304**, 679–681 (2012).
38. M. B. Cachón-González *et al*., The hairless gene of the mouse: Relationship of phenotypic effects with expression profile and genotype. *Dev. Dyn.* **216**, 113–126 (1999).
39. G. M. Beaudoin III, J. M. Sisk, P. A. Coulombe, C. C. Thompson, Hairless triggers reactivation of hair growth by promoting Wnt signaling. *Proc. Natl. Acad. Sci. U.S.A.* **102**, 14653–14658 (2005).
40. S. Fukada *et al*., Molecular signature of quiescent satellite cells in adult skeletal muscle. *Stem Cells* **25**, 2448–2459 (2007).
41. B. K. Kennedy, N. R. Austriaco Jr, J. Zhang, L. Guarente, Mutation in the silencing gene SIR4 can delay aging in *S. cerevisiae*. *Cell* **80**, 485–496 (1995).
42. T. Smeal, J. Claus, B. Kennedy, F. Cole, L. Guarente, Loss of transcriptional silencing causes sterility in old mother cells of *S. cerevisiae*. *Cell* **84**, 633–642 (1996).
43. B. Villeponteau, The heterochromatin loss model of aging. *Exp. Gerontol.* **32**, 383–394 (1997).
44. A. Brandt, G. Krohne, J. Grosshans, The farnesylated nuclear proteins KUGELKERN and LAMIN B promote aging-like phenotypes in Drosophila flies. *Aging Cell* **7**, 541–551 (2008).
45. E. Haithcock *et al*., Age-related changes of nuclear architecture in *Caenorhabditis elegans*. *Proc. Natl. Acad. Sci. U.S.A.* **102**, 16690–16695 (2005).
46. K. Larson *et al*., Heterochromatin formation promotes longevity and represses ribosomal RNA synthesis. *PLoS Genet.* **8**, e1002473 (2012).
47. P. Scaffidi, T. Misteli, Lamin A-dependent nuclear defects in human aging. *Science* **312**, 1059–1063 (2006).
48. M. M. Nava *et al*., Heterochromatin-driven nuclear softening protects the genome against mechanical stress-induced damage. *Cell* **181**, 800–817.e22 (2020).
49. R. H. Zhang, R. N. Judson, D. Y. Liu, J. Kast, F. M. Rossi, The lysine methyltransferase Ehmt2/G9a is dispensable for skeletal muscle development and regeneration. *Skelet. Muscle* **6**, 22 (2016).
50. L. Liu, T. H. Cheung, G. W. Charville, T. A. Rando, Isolation of skeletal muscle stem cells by fluorescence-activated cell sorting. *Nat. Protoc.* **10**, 1612–1624 (2015).
51. J. D. Buenrostro, P. G. Giresi, L. C. Zaba, H. Y. Chang, W. J. Greenleaf, Transposition of native chromatin for fast and sensitive epigenomic profiling of open chromatin, DNA-binding proteins and nucleosome position. *Nat. Methods* **10**, 1213–1218 (2013).
52. J. D. Buenrostro, B. Wu, H. Y. Chang, W. J. Greenleaf, ATAC-seq: A method for assaying chromatin accessibility genome-wide. *Curr. Protoc. Mol. Biol.* **109**, 21–29 (2015).
53. B. M. Gyori, G. Venkatachalam, P. S. Thiagarajan, D. Hsu, M. V. Clement, OpenComet: An automated tool for comet assay image analysis. *Redox Biol.* **2**, 457–465 (2014).